Arakelian 564: An XMM-*Newton* view

Cristian Vignali,[1,2]* W. N. Brandt,[1]* Th. Boller,[3]* A. C. Fabian[4]* and
Simon Vaughan[4,5]*

[1] *Department of Astronomy and Astrophysics, The Pennsylvania State University, 525 Davey Laboratory, University Park, PA 16802, USA*
[2] *INAF – Osservatorio Astronomico di Bologna, Via Ranzani 1, 40127 Bologna, Italy*
[3] *Max-Planck-Institut für extraterrestrische Physik, Postfach 1312, 85741 Garching, Germany*
[4] *Institute of Astronomy, Madingley Road, Cambridge, CB3 0HA*
[5] *Department of Physics and Astronomy, University of Leicester, Leicester, LE1 7RH*

ABSTRACT

We report on two XMM-*Newton* observations of the bright narrow-line Seyfert 1 galaxy
Ark 564 taken one year apart (2000 June and 2001 June). The 0.6–10 keV continuum is
well described by a soft blackbody component ($kT \approx 140$–150 eV) plus a steep power
law ($\Gamma \approx 2.50$–2.55). No significant spectral changes are observed between the two
observations, although the X-ray flux in the second observation is ≈ 40–50 per cent
lower. In both observations we detect a significant absorption edge at a rest-frame
energy of ≈ 0.73 keV, corresponding to O VII. The presence of the absorption feature
is confirmed by a simultaneous *Chandra* grating observation in 2000 June, although
the best-fitting edge threshold is at a slightly lower energy in the *Chandra* data,
possibly because of a different parameterisation of the underlying X-ray continuum.
We find tentative evidence for a broad iron emission line in the 2000 June observation.
The results from an analysis of the power spectral density (PSD) function are also
presented. The present XMM-*Newton* data support the idea that the PSD shows two
breaks, although the location of the high-frequency break requires further constraints.

Key words: galaxies: active — galaxies: individual: Ark 564 — galaxies: Seyfert —
X-rays: galaxies

1 INTRODUCTION

Narrow-Line Seyfert 1 galaxies (NLS1s) are a sub-class of active galactic nuclei (AGNs) defined by their exceptionally narrow optical permitted emission lines (Hβ FWHM < 2000 km s^{-1}) and their generally high Fe II/Hβ ratios (e.g., Osterbrock & Pogge 1985; Goodrich 1989), in comparison with "normal" broad-line Seyfert 1 galaxies (BLS1s). NLS1s often show extreme AGN properties; their ultraviolet (UV)/optical emission lines place them at one extreme of the Boroson & Green (1992) primary eigenvector. In the X-ray regime, NLS1s are characterized by rapid and large-amplitude variability (e.g., Boller, Brandt & Fink 1996; Boller et al. 1997); the normalised excess variance of variability is systematically larger in NLS1s than in BLS1s (e.g., Leighly 1999a; Turner et al. 1999; Cancelliere & Comastri 2002), despite both classes having sim-

ilar X-ray luminosity distributions. The X-ray spectra of NLS1s below ≈ 1–1.5 keV often show a prominent soft excess, modeled either by a steep power law or a thermal component (e.g., Brandt 1999; Comastri 2000). Moreover, their hard (> 2 keV) X-ray spectra are generally characterized by steeper power-law photon indices (e.g., Brandt, Mathur & Elvis 1997; Comastri 2000) than those of BLS1s. A likely explanation for the different properties of NLS1s is that they have relatively low masses for their central black holes and high accretion rates (e.g., Czerny et al. 2001; Boroson 2002; Wang & Netzer 2003). Smaller black hole masses can naturally explain both the narrowness of the optical emission lines, which are generated in gas that has smaller Keplerian velocities, and the extreme X-ray variability, since the primary emission would originate in a smaller region around the central engine. Soft photons from the accretion disc may Compton cool electrons in the corona and cause the steep observed photon indices (Pounds, Done & Osborne 1995; Haardt, Maraschi & Ghisellini 1997). In the case of high accretion rates, the surface of the disc is expected to be ionised (e.g., Matt, Fabian & Ross 1993; Ballantyne, Iwa-

* E-mail: chris@nellie.astro.psu.edu (CV); niel@astro.psu.edu (WNB); bol@xray.mpe.mpg.de (TB); acf@ast.cam.ac.uk (ACF); sav2@star.le.ac.uk (SV).

Table 1. Ark 564: XMM-*Newton* observations and source statistics.

	RGS1	RGS2	pn	MOS1	MOS2
Obs. ID=0006810201; Rev=96; Obs. Date=2000 June 17					
Exp. Time (ks)	5.59	5.43	......	......	......
Source Counts	15929	14111	......	......	......
Obs. ID=0006810101; Rev=96; Obs. Date=2000 June 17					
Exp. Time (ks)	11.68	11.47	6.10	6.30	6.53
Source Counts	25449	23401	307660	72359	80861
Obs. ID=0006810401; Rev=275; Obs. Date=2001 June 9					
Exp. Time (ks)	6.94	6.30	......	......	......
Source Counts	9002	8871	......	......	......
Obs. ID=0006810301; Rev=275; Obs. Date=2001 June 9					
Exp. Time (ks)	3.93	4.10	3.68	5.87	5.84
Source Counts	4463	4546	111450	43454	43719

The reported exposure times refer to the "cleaned" intervals (after removing the periods of flaring background) in the 0.3–2 keV band for the RGS and in the 0.3–10 keV band for the EPIC pn and MOS.

sawa & Fabian 2001). The disc will thus produce ionised Fe Kα features, as have apparently been observed from some NLS1s (e.g., Comastri et al. 1998; 2001; Vaughan et al. 1999b; Leighly et al. 1999b; Turner et al. 2001a).

Arakelian 564 (hereafter Ark 564; $z = 0.0247$) is one of the X-ray brightest NLS1s (e.g., Brandt et al. 1994; Vaughan et al. 1999a,b). In 2000 June it was the subject of an intensive multiwavelength monitoring campaign that included simultaneous observations with *ASCA* (Turner et al. 2001b, hereafter T01; Edelson et al. 2002), *RXTE* (Pounds et al. 2001), *Chandra* (Matsumoto, Leighly & Marshall 2001; Marshall 2002), XMM-*Newton* (this paper), *FUSE* (Romano et al. 2002), and *HST* (Collier et al. 2001; Crenshaw et al. 2002). Ark 564 represents a good target for XMM-*Newton*: the low-energy coverage allows accurate modeling of the soft excess, while the relatively large effective area at high energies allows studies of the previously revealed Fe Kα emission line (e.g., Comastri et al. 2001). Furthermore, the large XMM-*Newton* count rate allows the best possible studies of rapid variability.

2 DATA REDUCTION

Ark 564 was observed by XMM-*Newton* (Jansen et al. 2001) on 2000 June 17 (rev. 96) and 2001 June 9 (rev. 275).[1] At the beginnings of both observations the European Photon Imaging Camera (EPIC) instruments [pn (Strüder et al. 2001) and MOS (Turner et al. 2001)] were closed, while the Reflection Grating Spectrometer (RGS; den Herder et al. 2001) and the Optical Monitor (OM; Mason et al. 2001)

---

[1] Ark 564 was observed twice because of operational difficulties that prevented the entire accepted exposure from being obtained in one observation.
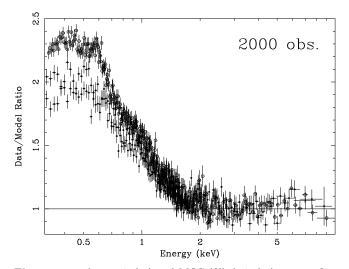
were operated. The EPIC cameras were operated in "Small-Window" mode to mitigate "pile-up" of photons from the source; EPIC data were acquired using the medium optical blocking filter. The data were reduced with the latest version of the XMM-*Newton* Science Analysis Software (SAS; version 5.4.1) using the latest calibration products. The data were filtered to avoid background flares (due to ≈ 100 keV protons; e.g., De Luca & Molendi 2002) which affect large intervals ($\approx 50\%$) of our observations. For the EPIC data, the tasks EPPROC and EMPROC were used to generate valid photon list. Both single-pixel and double-pixel events (patterns 0–4) were used when extracting the pn counts, while patterns 0–12 were used for the MOS. Source counts were extracted in the 0.3–12 keV band from circular regions of radius $90''$ (pn) and $50''$ (MOS); background counts were extracted from off-source regions of radius $45''$ (pn) and $150''$ (MOS). The statistics are clearly dominated by the source counts in any chosen EPIC sub-band. Response functions for spectral fitting to the EPIC data were generated using the tasks RMFGEN and ARFGEN. First-order RGS spectra were extracted using the RGSPROC task, which also produced the appropriate response matrices. A summary of the XMM-*Newton* observations of Ark 564 along with the source counts are presented in Table 1. Note the large numbers of counts obtained with the present XMM-*Newton* observations of Ark 564; for comparison, each *ASCA* Solid-state Imaging Spectrometer gathered $\approx 2 \times 10^6$ source counts over the whole 35-day observation (T01) and ≈ 12000 in the same time interval as the XMM-*Newton* observation (see §3.1).

3 SPECTRAL ANALYSIS

The source counts were grouped into spectra such that each spectral bin contained at least 20 counts to allow χ^2 fitting. X-ray spectra were fitted using the XSPEC package (version 11.2; Arnaud 1996). The quoted errors on derived model parameters correspond to the 90 per cent confidence level for one interesting parameter (i.e., $\Delta\chi^2 = 2.71$; Avni 1976) unless otherwise stated. All spectral fits include absorption due to the line-of-sight Galactic column density of $N_H = 6.4 \times 10^{20}$ cm^{-2} (Dickey & Lockman 1990). Hereafter we adopt H_0=70 km s^{-1} Mpc^{-1} in a Λ-cosmology with Ω_M=0.3 and Ω_Λ=0.7.

At first the MOS1 and MOS2 spectra were fitted separately to check for cross-calibration uncertainties; these have been found to be $\approx 3\%$ (Kirsch 2003). We found generally good agreement between MOS1 and MOS2, comparable with the value quoted above. Therefore in the following we will present the spectral results of both cameras referred to as MOS.

Cross-calibration uncertainties between pn and MOS are generally at most $\approx 13\%$ (Kirsch 2003). However, the pn and MOS spectra of Ark 564 in both observations clearly differ at energies below ≈ 0.6 keV; this is probably due to residual calibration problems in the "Small-Window" mode. A similar difference in the pn/MOS behaviour at low energies has been found for PG 1211+143 (see Fig. 3 of Pounds et al. 2003). Therefore, in the following the pn and MOS data will be fitted together with the same model in the 0.6–10 keV band, leaving the relative normalisations free to vary. We note, however, that some discrepancies between the pn and

Figure 1. pn (open circles) and MOS (filled circles) spectra fitted above 2 keV with a power law with $\Gamma \approx 2.5$ that has been extrapolated back to lower energies. An excess of counts is clearly seen below ≈ 1.5 keV in all EPIC instruments.

MOS seem to be present up to ≈ 0.9 keV. The extension of our analysis down to 0.3 keV has the advantage of providing a slightly better constraint on the temperature of the soft thermal component without changing our main results.

3.1 Spectral results: The 2000 June observation

A single power-law model provides a poor fit to the 0.6–10 keV pn+MOS data; strong residuals at low energies are evident in both instruments, as shown in Fig. 1. The soft excess of Ark 564 rises sharply below ≈ 1.5 keV similarly to the *BeppoSAX* observation (see Fig. 6 of Comastri et al. 2001). The presence of a soft component, parameterised either by a blackbody or a power law, is common across the NLS1 population (e.g., Comastri 2000; Vaughan et al. 2002). If thermal, this component is usually ascribed to the high-energy tail of the accretion disc responsible for the UV bump detected in the majority of NLS1s (see, e.g., Soria & Puchnarewicz 2002 for discussion), although the rapid variability of the soft component detected from some NLS1s casts doubts on simple versions of the accretion-disc interpretation. Fitting the soft excess with a power law is inadequate; there is clear continuum spectral curvature that is not accounted for by a power law. Spectral curvature with similar shape has been detected in some other Seyfert galaxies (see, e.g., Pounds & Reeves 2002 for a review; Collinge et al. 2001) and also in the narrow emission-line quasar PG 1211+143 (Pounds et al. 2003). The addition of a blackbody component is preferred by the EPIC data and finds support from previous *BeppoSAX* results (Comastri et al. 2001). This component has $kT = 138^{+2}_{-3}$ eV [see model (1) in Table 2]. At higher energies, a power law with photon index $\Gamma = 2.55 \pm 0.02$ dominates the spectrum. This model leaves significant residuals at soft X-ray energies. The shape of these residuals (see Fig. 2) indicates a count deficit at ≈ 0.7 keV. We therefore added an absorption edge to the previous model [see model (2) in Table 2]. The edge provides a highly significant improvement in the fit quality ($\Delta\chi^2/\Delta$d.o.f.=163/2). Its rest-frame threshold energy,

Table 2. 2000 June observation: EPIC pn+MOS spectral results.

Model	kT (eV)	Γ	E_{edge} (eV)	τ	$\chi^2/d.o.f.$
(1)	138^{+2}_{-3}	2.55 ± 0.02	....	....	1244/902
(2)	148^{+2}_{-3}	2.52 ± 0.02	731 ± 11	$0.38^{+0.07}_{-0.06}$	1081/900

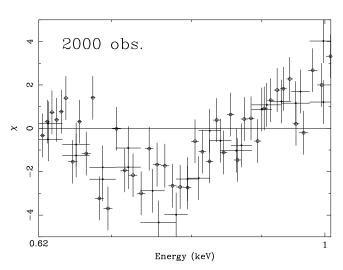The edge threshold energy is in the source rest frame.

Figure 2. Soft X-ray data-to-model residuals (in terms of σ with error bars of size one) obtained when the pn+MOS data are fitted with a blackbody plus power-law model [model (1) in Table 2]. Symbols are the same as in Fig. 1.

731 ± 11 eV, is consistent with the edge being due to O VII (which has an energy of 739 eV). The 68, 90, and 99 per cent confidence contours for the edge energy vs. optical depth (in the observed frame) are shown in Fig. 3. The edge is still required when other continuum models for the soft component (e.g., a power law, a double blackbody) are chosen, although the fit is significantly worse.

The edge is also present in the *Chandra* High-Energy Transmission Grating (HETG) data taken simultaneously with the XMM-*Newton* observation (see the spectrum shown in Fig. 3 of Matsumoto et al. 2001). The edge rest-frame threshold energy in the *Chandra* observation (712^{+3}_{-4} eV; Matsumoto et al. 2001; Marshall 2002) is not in agreement with the nominal energy of the O VII K-edge. The hypothesis that *Chandra* observed a highly redshifted O VII K-edge with a velocity of ≈ 1000 km s^{-1} appears unlikely since the O VII absorption lines detected by *Chandra* have no measurable velocity shifts (Matsumoto et al. 2001). We have performed an analysis of the RGS data searching for the spectral features reported by Matsumoto et al. (2001) based upon HETG data. However, we do not find any clear absorption lines (at most $\Delta\chi^2/\Delta$d.o.f.=10/2 for a narrow absorption line) despite the high counting statistics of the RGS data. This is presumably due to the lower spectral resolution of the RGS; the HETG spectral features are unresolved even with the higher spectral resolution of the HETG. Therefore, below we use the RGS mainly to check the results derived from the EPIC spectral fitting rather than presenting a detailed analysis of the RGS data. The edge is also
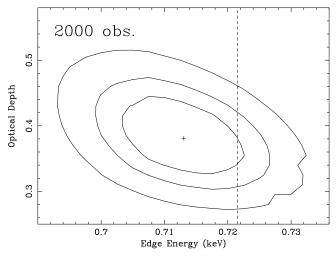
Figure 3. 68, 90, and 99 per cent confidence contours for the edge energy (in the observed frame) vs. optical depth. The dashed vertical line shows the redshifted energy of the O VII K-edge.

Figure 4. Best-fitting spectrum [model (2) in Table 2] for the EPIC 2000 June data. The data-to-model residuals are shown in the bottom panel in units of σ. Symbols are the same as in Fig. 1.

present in the RGS spectra, although at a much lower significance level; spectral simulations suggest that this result is due to the combination of lower statistics and the presence of chip gaps in the RGS. The underlying continuum measured by the HETG is well parameterised by a model similar to the one used for our XMM-*Newton* observation, even though the HETG bandpass is significantly narrower than the XMM-*Newton* one. While the HETG best-fitting photon index ($\Gamma = 2.56 \pm 0.06$) is consistent with the one measured by XMM-*Newton*, the blackbody component has a lower temperature ($kT = 124 \pm 3$ eV). The different blackbody temperature may be the cause of the different edge energy in the HETG observation.

Adopting the blackbody plus power-law model and adding a warm absorber (ABSORI in XSPEC; Magdziarz & Zdziarski 1995) to fit the absorption feature of Ark 564 does not provide good results; significant residuals are still present at the energy corresponding to the O VII edge. The ionisation parameter, defined as $\xi = \frac{L}{nR^2}$, where L is the source luminosity, n the warm absorber density, and R the distance of the absorber from the photoionising source, is 73^{+43}_{-35} erg cm s^{-1}. For reasonable assumptions of the physical parameters, the strongest bound-free soft X-ray absorption features in the warm absorber model are the O VII and O VIII K-edges (e.g., Reynolds & Fabian 1995; Reynolds 1997; George et al. 1998). The relatively large optical depth of the detected O VII edge probably causes the failure of the warm absorber model, since ABSORI also predicts the presence of the O VIII edge which is not observed in the data ($\tau < 0.08$). Although data with better resolution and higher signal-to-noise ratio are required to provide a physical justification for the presence of the O VII edge and the absence or weakness of the O VIII edge, we note that similar spectral results have been found for the Seyfert 1 galaxy H 1419+480 using XMM-*Newton* data (Barcons, Carrera & Ceballos 2003). Although the different spectral resolution does not allow a proper comparison of the absorption features at different wavelengths, there are claims that the UV and X-ray absorbers in Ark 564 are physically related and possibly identical (e.g., Romano et al. 2002; Crenshaw et al.
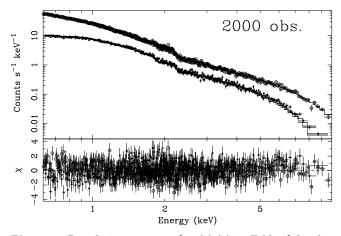
1999, 2002; Matsumoto, Leighly & Marshall 2002). However, the $N_{\text{O VII}}$ value we derive from the observed K-edge optical depth ($\approx 1.4 \times 10^{18}$ cm^{-2}) is about an order of magnitude larger than the value predicted in Table 4 of Crenshaw et al. (2002) using photoionisation models and assuming the UV absorber to be a single zone. It is likely that a more complex structure for the absorber is required to reproduce both the UV and X-ray data.

In 2000 June Ark 564 was also observed by *ASCA* (T01) with a 35-day observation (from 2000 June 1 to July 6). Unfortunately, the lower statistics in the portion of *ASCA* data (re-analysed using standard procedures; ≈ 12000 counts per instrument) taken simultaneously with our XMM-*Newton* observation and the exclusion of the data below 0.7 keV do not allow one to reveal the O VII edge detected by XMM-*Newton*.[2] However, the spectral parameters for the blackbody ($kT = 146 \pm 9$ eV) and the power-law ($\Gamma = 2.46 \pm 0.03$) components are in relatively good agreement with our results.

At high X-ray energies, the long *ASCA* observation indicates that the iron Kα emission line is complex, best fitted using a relativistic iron line produced by an accretion disc in either the Schwarzschild or Kerr metrics (XSPEC models DISKLINE and LAOR, respectively; Fabian et al. 1989; Laor 1991), and variable on time scales of a few days. The analysis of the *ASCA* data exactly simultaneous with our XMM-*Newton* observation, however, indicates only marginal evidence ($\Delta\chi^2/\Delta$d.o.f.=6/2) for an ionised Fe Kα line (EW=113^{+181}_{-79} eV). This is possibly caused by the relatively poor statistics in the short time interval simultaneous with the XMM-*Newton* observation. The addition of a narrow ($\sigma = 10$ eV) emission line improves the EPIC fit quality by $\Delta\chi^2$=8 at most when all of the line parameters, except for its normalisation, are frozen. We obtain EW=32^{+46}_{-17} eV, EW=35^{+30}_{-31} eV, and EW=43^{+36}_{-35} eV for the neutral (6.40 keV), He-like (6.70 keV), and H-like (6.97 keV) Fe Kα lines, respectively. We tried to account for the small residuals at high energies, having a "bump-like" shape (see Fig. 4), using a relativistic iron line pro-

---

[2] See §2 of T01 for a discussion of the *ASCA* calibration problems that led the authors to avoid the spectral band below 0.7 keV.

duced by an accretion disc. The DISKLINE model improves the fit by $\Delta\chi^2/\Delta d.o.f.=12/2$ when all the line parameters are frozen to the default values[3] excluding the line energy and its normalisation, which are left free to vary. The line rest-frame energy is $6.10^{+0.31}_{-0.17}$ keV, while its intensity is EW=98^{+48}_{-46} eV. Both the line energy and EW are lower than the values found by T01. This is probably due to the fact that this model fails in reproducing the peak of the residuals at ≈ 7 keV in the present XMM-*Newton* data. Using the LAOR model[4] the improvement is slightly more significant ($\Delta\chi^2/\Delta d.o.f.=18/2$). The line rest-frame energy, considerably higher ($7.07^{+0.27}_{-0.20}$ keV) than in the previous model, and its EW (471^{+175}_{-86} eV) are consistent with the best-fit model of T01, where the line peaks at ≈ 7 keV. However, in contrast with the *ASCA* results shown by T01, the presence of a complex Fe Kα line is not strongly motivated by the present XMM-*Newton* data, either by the residuals to a power-law fit or by the improvement in the χ^2 after the inclusion of this feature. It is possible that residual uncertainties either in the calibration of XMM-*Newton* spectra at high energies in "Small-Window" mode or in *ASCA*, coupled with a rapid change in the intensity and shape of the line (already probed by the longer *ASCA* observation), are responsible for the different results we obtained. Further investigations on this issue are required.

When a reflection component is added to the blackbody plus power-law model, a much steeper photon index is obtained (as expected, given the known correlation of these parameters in the reflection models available in XSPEC; see Vaughan & Edelson 2001 and Perola et al. 2002 for discussion), but the fit does not improve significantly. The generally flatter photon index in MOS1 data (see Molendi & Sembay 2003) and, possibly, problems in the pn-MOS cross-calibration using the "Small-Window" mode could produce a spurious reflection component in the MOS data. The significantly higher statistics collected by the EPIC pn at high energies reveal no evident additional spectral components and indicate that model (2) in Table 2 is a good parameterisation of the Ark 564 spectrum in the 2000 June observation. However, motivated by the discoveries of sharp drops in the XMM-*Newton* spectra of two other NLS1s, 1H 0707−495 (Boller et al. 2002) and IRAS 13224−3809 (Boller et al. 2003), we fitted the 2–10 keV data using the best-fitting power law obtained in the 2–7 keV band (thus avoiding any problems with the O VII edge and the soft thermal component). In contrast with the results obtained for the other two NLS1s, we find only marginal evidence for a drop at ≈ 7–8 keV ($\Delta\chi^2/\Delta d.o.f.=6/2$) when the drop is parameterised by an absorption edge). This is a further indication that the present XMM-*Newton* data do not require more complex modeling at high energies.

[3] We assumed the line originates between 10 and 1000 gravitational radii and adopted an emissivity law r^{-q} with $q = 2$ for the illumination pattern of the accretion disc; the inclination angle of the disc was fixed to $30°$.
[4] We fixed the innermost radius as the last stable orbit for a Kerr black hole and the outer radius at the maximum value allowed by the model (400 gravitational radii). We fixed the emissivity index to 3 and the inclination angle of the disk to $30°$.

Table 3. 2001 June observation: EPIC pn+MOS spectral results.

Model	kT (eV)	Γ	E_{edge} (eV)	τ	$\chi^2/d.o.f.$
(1)	136±3	2.56±0.03	....	....	968/757
(2)	144^{+4}_{-3}	2.54±0.03	727^{+15}_{-16}	$0.45^{+0.13}_{-0.06}$	900/755

The edge threshold energy is in the source rest frame.
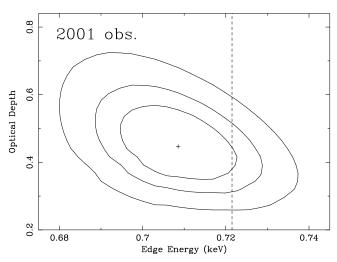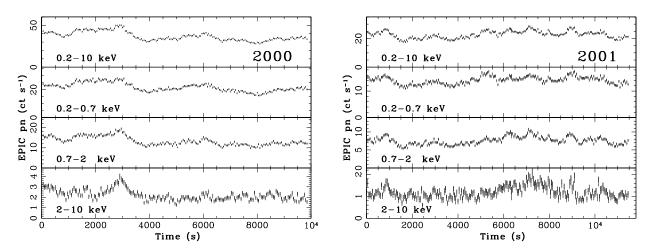

Figure 5. 68, 90, and 99 per cent confidence contours for the edge energy (in the observed frame) vs. optical depth. The dashed vertical line shows the redshifted energy of the O VII K-edge.

3.2 Spectral results: The 2001 June observation

The 2001 June XMM-*Newton* EPIC observation of Ark 564 is characterized by lower statistics (see Table 1) than the 2000 June observation. The exposure time, after the screening procedure, is relatively low, and the source has a lower flux level (see §4). Following §3.1, a blackbody plus power law is used to model the broad-band X-ray continuum of Ark 564; the blackbody temperature and the power-law photon index [see model (1) in Table 3] are consistent with the corresponding model in the 2000 June observation (see Table 2). The poor quality of the fit, however, is suggestive of additional spectral complexity, in particular below ≈ 1 keV. Based on the 2000 observation and the shape of the residuals in the 2001 observation, we tried to account for the poor spectral fit by adding an absorption edge [model (2) in Table 3]. The edge is significant statistically ($\Delta\chi^2/\Delta d.o.f.=68/2$); its rest-frame threshold energy, 727^{+15}_{-16} eV, is consistent with the O VII K-edge (see Fig. 5), as in the 2000 June observation, and also the edge optical depth agrees with the previous EPIC observation. Some indications of this spectral feature are also present in the RGS data. There is no clear evidence for additional spectral features in the 2001 XMM-*Newton* data. An upper limit of $\tau = 0.12$ is derived for the O VIII optical depth; adopting a warm absorber model to reproduce the O VII edge provides a worse spectral fit and a poorly constrained ionisation parameter.

Although in the 2001 June observation of Ark 564 the hard X-ray photon statistics are limited, we can place

Figure 6. 2000 (left panel) and 2001 (right panel) pn light curves (50-s time bins). From top to bottom: 0.2–10 keV, 0.2–0.7 keV, 0.7–2 keV, and 2–10 keV. The count rate has not been scaled for detector efficiency ($\approx 71\%$ in "Small-Window" mode).

some constraints on the presence of Fe Kα emission lines (both neutral and ionised). We find marginal evidence ($\Delta\chi^2/\Delta$d.o.f.=12/2; the width of the line is frozen to $\sigma = 10$ eV) for a Gaussian Fe Kα line. The line rest-frame energy ($6.16^{+0.05}_{-0.02}$ keV), lower than that expected for the neutral Fe Kα emission line, coupled with its low significance casts some doubts on the nature of this feature. If we freeze the line energy at 6.40 keV, 6.70 keV, and 6.97 keV for the neutral, He-like, and H-like Fe Kα lines, we obtain EW< 71 eV, EW=70^{+60}_{-61} eV, and EW< 114 eV, respectively, but none of these features is significant statistically. The absence or weakness of iron lines is supported by the lack of a strong reflection component, as the relatively good fit obtained at high energies with model (2) also suggests.

4 FLUX VARIABILITY

Between the 2000 and 2001 observations, Ark 564 shows significant flux variability. In the 2000 June observation, the observed soft ($F_{0.5-2 \text{ keV}}$) and hard ($F_{2-10 \text{ keV}}$) band fluxes are $(4.7–5.4)\times10^{-11}$ erg cm^{-2} s^{-1} and $(2.1–2.4)\times10^{-11}$ erg cm^{-2} s^{-1}, respectively, depending on the EPIC camera used and adopting the best-fitting models reported in Table 2. These correspond to Galactic absorption-corrected luminosities of $(8.8–10.0)\times10^{43}$ erg s^{-1} and $(3.0–3.4)\times10^{43}$ erg s^{-1}, respectively. In 2001 June the source shows a flux level lower by $\approx$ 40–50 per cent. We found $F_{0.5-2 \text{ keV}}$=$(3.0–3.2)\times10^{-11}$ erg cm^{-2} s^{-1} and $F_{2-10 \text{ keV}}$=$(1.1–1.2)\times10^{-11}$ erg cm^{-2} s^{-1} [model (2) in Table 3], corresponding to intrinsic luminosities of $(5.7–6.0)\times10^{43}$ erg s^{-1} in the soft band and $(1.7–1.8)\times10^{43}$ erg s^{-1} in the hard band. In both observations, the presence of a larger luminosity in the soft band than in the hard band argues against a simple model where the soft excess is just due to reprocessed hard X-ray emission.

For each observation, pn light curves were extracted in the 0.2–10 keV range for continuous periods of 9.9 and 11.5 ks from the 2000 and 2001 data sets, respectively, and binned to 50-s time resolution (see Fig. 6, top panels).[5] The light curves were background subtracted and exposure corrected (i.e., corrected for telemetry drop outs). Analyses of the pn light curves in different energy bands (0.2–10 keV, 0.2–0.7 keV, 0.7–2 keV, and 2–10 keV; see Fig. 6) show that the source is highly variable, both at low and high energies. The rapid variability of the soft component and its relatively high temperature (see §3.1 and 3.2) suggest that it is unlikely to be simple thermal radiation from an accretion disc. It is possible that it is quasi-thermal emission originally from the accretion disc that has been upscattered in a hot surface layer of the disc or the corona. Alternatively, the soft component might be due to turbulent Comptonisation occurring close to the black hole (Socrates, Davis & Blaes 2003).

5 POWER SPECTRAL DENSITY FUNCTION

The high-frequency power spectral density function (PSD) of Ark 564 was estimated from the pn light curves using the method of Vaughan, Fabian & Nandra (2003). pn 2000 and 2001 periodograms were computed using standard Fourier methods. The two periodograms appeared consistent with one another, and therefore a single binned periodogram was produced by combining the two periodograms and binning, using the method of Papadakis & Lawrence (1993), such that there are 15 periodogram estimates per frequency bin. Figure 7 shows the average periodogram. At high frequencies the power is dominated by the Poisson noise. At low frequencies the source variations dominate with a steep, approximately power-law spectrum rising toward low frequencies.

---

[5] We used the total (whole interval) light curves irrespective of the periods of "flaring background" because the source count rate is much higher than the background even during the flares. The background flares are weak compared to many seen by XMM-*Newton*, and the exclusion of these intervals for the spectral analysis was conservative. Their effect on the PSD derived in §5 is negligible. Similarly, the exclusion of the 0.2–0.3 keV data from the spectral analysis was a conservative choice.
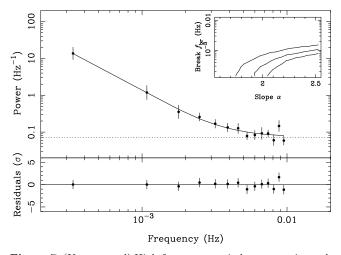
Figure 7. (Upper panel) High-frequency periodograms estimated using the 0.2–10 keV light curves and 50-s resolution. The solid curve shows the best-fitting model; the background noise level (from Poisson noise) is indicated with the dotted line. The 68, 90, and 99 per cent confidence contours for the two interesting parameters (the power-law index and the break frequency) are shown in the insert. (Lower panel) Data-to-model residuals in units of σ.

From previous monitoring with *RXTE* and *ASCA* it is known that the low-frequency PSD is well represented by a broken power law, with a power-law index of ≈ 0 below a frequency $f_{br} \approx 1.6 \times 10^{-6}$ Hz and an index of ≈ 1.2 above the break (Markowitz et al. 2003). The XMM-*Newton* data at much higher frequencies show a much steeper spectrum and imply the PSD must show a high-frequency break as well, confirming the suggestion of Papadakis et al. (2002) on the basis of *ASCA* data. In order to estimate the high-frequency PSD, these data were fitted using the Monte Carlo procedure of Vaughan et al. (2003) with a doubly broken power-law model. The power spectral index was fixed at 0 below 10^{-6} Hz and 1.2 above this frequency. Then a second, high-frequency break was included in the model with both the break frequency (f_{br}) and the spectral index above the break (α) as free parameters in the fitting.[6]

This model provided a statistically acceptable fit to the data ($\chi_\nu^2 < 1.0$), but the free parameters were poorly constrained. The PSD is steep, with an index $\alpha > 1.95$, but the location of the break to this steep slope is only constrained to be $f_{br} < 8 \times 10^{-4}$ Hz (90 per cent confidence limit for one interesting parameter). This fit thus supports the claim by Papadakis et al. (2002) that Ark 564 shows a doubly broken PSD, although the inferred position of the break is a factor ≈ 2 lower than that obtained in their analysis.

Curiously, the doubly broken PSD resembles that seen in Cyg X-1 in its low/hard state, contrary to the expectation that Ark 564 might look more like the high/soft state (which only shows the high-frequency break). However, it is vital to constrain the high-frequency PSD and to confirm the second break in the PSD before a fair comparison can be made

---

[6] The low-frequency PSD needed to be specified in the model as the fitting procedure accounts for biases in the periodogram, notably "red-noise leak", that depend on the PSD at low frequencies. See Vaughan et al. (2003) for details on this.

between Ark 564 and Galactic black hole candidates (which can also show "very high" and "intermediate" state PSDs).

6 SUMMARY

We have reported two XMM-*Newton* observations of the bright NLS1 Ark 564 taken one year apart. The principal results are the following:

- A blackbody with $kT \approx 140$–150 eV and a power law with $\Gamma \approx 2.50$–2.55 provide a good parameterisation of the X-ray continuum. No significant spectral changes are observed between the two observations, although the X-ray flux in the second observation is lower by ≈ 40–50 per cent.
- In both observations a significant absorption edge at ≈ 0.73 keV, corresponding to the O VII K-edge, is detected.
- We find tentative evidence for an iron emission line (fitted using a LAOR model) in the 2000 June observation.
- The present XMM-*Newton* data support the idea that the PSD shows two breaks. A longer observation is required to place stronger constraints on the location of the high-frequency break.

REFERENCES

Arnaud K.A., 1996, in Jacoby G., Barnes J., eds, ASP Conf. Ser. Vol. 101, Astronomical Data Analysis Software and Systems V. Astron. Soc. Pac., San Francisco, 17
Avni Y., 1976, ApJ, 210, 642
Ballantyne D.R., Iwasawa K., Fabian A.C., 2001, MNRAS, 323, 506
Barcons X., Carrera F.J., Ceballos M.T., 2003, MNRAS, in press (astro-ph/0304210)
Boller Th., Brandt W.N., Fink H.H., 1996, A&A, 305, 53
Boller Th., Brandt W.N., Fabian A.C., Fink H.H., 1997, MNRAS, 289, 393
Boller Th. et al., 2002, MNRAS, 329, 1
Boller Th., Tanaka Y., Fabian A.C., Brandt W.N., Gallo L., Anabuki N., Haba Y., Vaughan S., 2003, MNRAS, 343, L89
Boroson T.A., 2002, ApJ, 565, 78
Boroson T.A., Green R.F., 1992, ApJS, 80, 109
Brandt W.N., 1999, in Poutanen J., Svensson R., eds, High Energy Processes in Accreting Black Holes, Astron. Soc. Pac., San Francisco, 166

Brandt W.N., Fabian A.C., Nandra K., Reynolds C.S., Brinkmann W., 1994, MNRAS, 271, 958

Brandt W.N., Mathur S., Elvis M., 1997, MNRAS, 285, L25

Cancelliere F., Comastri A., 2002, "Inflows, Outflows and Reprocessing around black holes", proceedings of 5th Italian AGN Meeting, electronic publication (astro-ph/0301163)

Collier S. et al., 2001, ApJ, 561, 146

Collinge M.J. et al., 2001, ApJ, 557, 2

Comastri A., 2000, New Astronomy Review, 44, 403

Comastri A. et al., 1998, A&A, 333, 31

Comastri A. et al., 2001, A&A, 365, 400

Crenshaw D.M., Kraemer S.B., Boggess A., Maran S.P., Mushotzky R.F., Wu C.-C., 1999, ApJ, 516, 750

Crenshaw D.M. et al., 2002, ApJ, 566, 187

Czerny B., Nikołajuk M., Piasecki M., Kuraszkiewicz J., 2001, MNRAS, 325, 865

De Luca A., Molendi S., 2002, in New Visions of the X-ray Universe in the XMM-*Newton* and *Chandra* era, in press (astro-ph/0202480)

den Herder J.W. et al., 2001, A&A, 365, L7

Dickey J.M., Lockman F.J., 1990, ARA&A, 28, 215

Edelson R., Turner T.J., Pounds K.A., Vaughan S., Markowitz A., Marshall H., Dobbie P., Warwick R., 2002, ApJ, 568, 610

Fabian A.C., Rees M.J., Stella L., White N.E., 1989, MNRAS, 238, 729

George I.M., Turner T.J., Netzer H., Nandra K., Mushotzky R.F., Yaqoob T., 1998, ApJS, 114, 73

Goodrich R.W., 1989, ApJ, 342, 224

Haardt F., Maraschi L., Ghisellini G., 1997, ApJ, 476, 620

Jansen F. et al., 2001, A&A, 365, L1

Kirsch M., 2003, XMM-*Newton* Users Group Meeting Presentations (CAL-TN-0018-2-1)

Laor A., 1991, ApJ, 376, 90

Leighly K.M., 1999a, ApJS, 125, 297

Leighly K.M., 1999b, ApJS, 125, 317

Magdziarz P., Zdziarski A.A., 1995, MNRAS, 273, 837

Markowitz A. et al., 2003, ApJ, 593, 96

Marshall H.L., 2002, in Boller Th., Komossa S., Kahn S., Kunieda H, Gallo L., eds, X-ray Spectroscopy of AGN with *Chandra* and XMM-*Newton*, MPE Report 279, Garching, 235

Mason K.O. et al., 2001, A&A, 365, L36

Matsumoto C., Leighly K.M., Marshall H.L., 2001, in Yaqoob T., Krolik J.H., X-ray Emission from Accretion onto Black Holes, JHU/LHEA Workshop, electronic publication (http://www.pha.jhu.edu/groups/astro/workshop2001/)

Matsumoto C., Leighly K.M., Marshall H.L., 2002, in Boller Th., Komossa S., Kahn S., Kunieda H, Gallo L., eds, X-ray Spectroscopy of AGN with *Chandra* and XMM-*Newton*, MPE Report 279, Garching, 263

Matt G., Fabian A.C., Ross R.R., 1993, MNRAS, 264, 839

Molendi S., Sembay S., 2003, XMM-*Newton* Calibration Presentations (CAL-TN-0036-1-0)

Osterbrock D.E., Pogge R.W., 1985, ApJ, 297, 166

Papadakis I.E., Lawrence A., 1993, MNRAS, 261, 612

Papadakis I.E., Brinkmann W., Negoro H., Gliozzi M., 2002, A&A, 382, L1

Perola G.C., Matt G., Cappi M., Fiore F., Guainazzi M., Maraschi L., Petrucci P.-O., Piro L., 2002, A&A, 389, 802

Pounds K.A., Done C., Osborne J.P., 1995, MNRAS, 277, L5

Pounds K.A., Edelson R., Markowitz A., Vaughan S., 2001, ApJ, 550, L15

Pounds K.A., Reeves J.N., 2002, in New Visions of the X-ray Universe in the XMM-*Newton* and *Chandra* era, in press (astro-ph/0201436)

Pounds K.A., Reeves J.N., King A.R., Page K.L., O'Brien P.T., Turner M.J.L., 2003, MNRAS, in press (astro-ph/0303603)

Reynolds C.S., 1995, MNRAS, 286, 513

Reynolds C.S., Fabian A.C., 1997, MNRAS, 273, 1167

Romano P., Mathur S., Pogge R.W., Peterson B.M., Kuraszkiewicz J., 2002, ApJ, 578, 64

Socrates A., Davis S.W., Blaes O., 2003, ApJ, submitted (astro-ph/0307158)

Soria R., Puchnarewicz E.M., 2002, MNRAS, 329, 456

Strüder L. et al., 2001, A&A, 365, L18

Turner M.J.L. et al., 2001, A&A, 365, L27

Turner T.J., George I.M., Nandra K., Turcan D., 1999, ApJ, 524, 667

Turner T.J. et al., 2001a, ApJ, 548, L13

Turner T.J., Romano P., George I.M., Edelson R., Collier S.J., Mathur S., Peterson B.M., 2001b, ApJ, 561, 131 (T01)

Vaughan S., Pounds K.A., Reeves J., Warwick R., Edelson R., 1999a, MNRAS, 308, L34

Vaughan S., Reeves J., Warwick R., Edelson R., 1999b, MNRAS, 309, 113

Vaughan S., Edelson R., 2001, ApJ, 548, 694

Vaughan S., Boller Th., Fabian A.C., Ballantyne D.R., Brandt W.N., Trümper J., 2002, MNRAS, 337, 247

Vaughan S., Fabian A.C., Nandra K., 2003, MNRAS, 339, 1237

Wang J.-M., Netzer H., 2003, A&A, 398, 927

This paper has been typeset from a TeX/ LaTeX file prepared by the author.